A 1.5 GHz WIDE-BAND BEAM-POSITION AND INTENSITY MONITOR FOR THE ELECTRON-POSITRON ACCUMULATOR (EPA)

G.C. Schneider,
CERN, 1211 Geneva 23, Switzerland

Abstract

This paper describes a resistive beam monitor which was developed and built for the observation of transverse and longitudinal microwave instabilities and for bunch length ($\sigma = 0.7$ ns) measurements. The relevant equations are derived, analysed, and optimized. The electrical and mechanical layouts are given and also the characteristics of the monitor. The signals for horizontal and vertical beam-position and intensity have a rise-time of ≤ 230 ps at the end of 100 m transmission cables. The cable losses are compensated by computer-optimized filters. The beam coupling impedance Z/n is max. 0.2 Ω. The peak intensity signal is 2.7 V for the nominal beam intensity of 2.5×10^{10} e^+/e^- particles per bunch. At 40 mm off centre, the position signals equal the intensity signal. A laboratory test set-up allows the transverse displacement of a rod or wire in a 3 m long, cylindrical chamber. Time filtering is used to avoid disturbances by imperfect matching at the end of the tube for off-centre wire positions. We present the results obtained with the laboratory test set-up and with actual e^- beam when the monitor was installed in the accumulator ring. Errors and limits are discussed.

1. Introduction

A charged-particle bunch moving with a highly relativistic speed in a well-conducting vacuum chamber is accompanied by a pure transverse electric field. The induced charge distribution of the image current on the chamber wall versus the beam position is well known:[1-4]

$$\boxed{q(r,\phi,\chi) = (1 - r^2)/[1 + r^2 - 2r\cos(\phi - \chi)]\ .} \tag{1}$$

The parameters are shown in Fig. 1, where the circular chamber is represented as the unit circle in the x-y plane. The beam position is given by the vector

$$r = |r|\, e^{j\chi}\ . \tag{2}$$

The charge density q appears over the azimuthal angle ϕ. Figure 2 shows q versus ϕ [Eq. (1)] for six beam positions r on the real axis ($\chi = 0$). The integral

$$\int_{-\pi}^{\pi} q(r,\phi)\, d\phi = 2\pi \tag{3}$$

is a constant for all beam positions r.

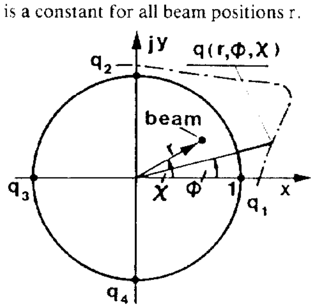

Fig. 1

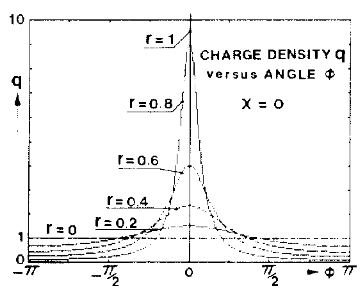

Fig. 2

2. Four-Point Pick-Up with Uniformly Conducting Ring

Knowledge of the chamber image current at the four axis points is sufficient to determine the beam position and the intensity. These four currents are measured by means of a resistive ring inserted in the vacuum chamber (see Fig. 5). The four voltages U_A, U_B, U_C, and U_D then appear over the resistive gap.

We consider the four charges q_ν ($\nu = 1, 2, 3, 4$) at the axis points where $\phi = 0, \pi/2, \pi$, and $(3/2)\pi$. Then from Eq. (1),

$$q_\nu = (1 - r^2)/\{1 + r^2 - 2r\cos[(\pi/2)(\nu - 1) - \chi]\}\ . \tag{4}$$

2.1 The difference charge between q_1 and q_3 [from Eq. (4)] is

$$\boxed{\Delta q_{13} = q_1 - q_3 = [(1 - r^2)4r\cos\chi]/[(1 + r^2)^2 - 4r^2\cos^2\chi]\ ,} \tag{5}$$

or in Cartesian coordinates with $x = r\cos\chi$ and $r^2 = x^2 + y^2$,

$$\boxed{\Delta q_{13}(x, y) = [(1 - x^2 - y^2)4x]/(1 + y^2 - 3x^2)\ .} \tag{6}$$

Figure 3 gives for illustration a three-dimensional presentation of Δq_{13}. The slope s is maximum (= 4) in the centre and decreases to the border $y = \pm 1$.

2.2 The sum of the four point-charges $\Sigma q = q_1 + q_2 + q_3 + q_4$ from Eq. (4) yields[5]

$$\boxed{\Sigma q(r,\chi) = [4(1 - r^8)]/[(1 - r^4)^2 + 16r^4\cos^2\chi \cdot \sin^2\chi]\ .} \tag{7}$$

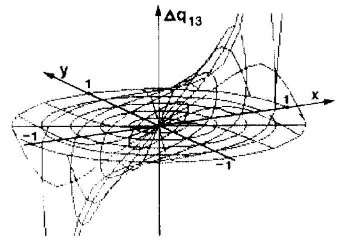

Fig. 3

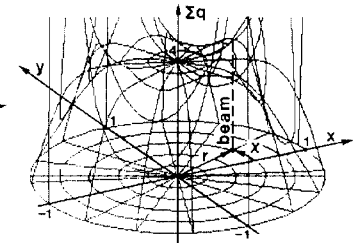

Fig. 4

Figure 4 shows a three-dimensional representation of Eq. (7); Σq is const = 4 for small r. The maximum error[5] is about 5% for $|r| \leq 0.4$.

2.3 The normalized beam-position signal can be found from Eqs. (5) and (7)

$$\boxed{\frac{\Delta q}{\Sigma q} = \frac{r\cos\chi\,[(1 - r^4)^2 + 16r^4\cos^2\chi\sin^2\chi}{[(1 + r^2)^2 - 4r^2\cos^2\chi](1 + r^2 + r^4 + r^6)}} \tag{8}$$

It has for small r a constant slope of 1 in the x direction.

2.4 The linearity error in the x direction with respect to the full scale $x_{max} = 1$,

$$\epsilon_f = [(\Delta q/\Sigma q) - x]/x_{max} = (\Delta q/\Sigma q) - r\cos\chi\ , \tag{9}$$

is also about 5% for $|r| \leq 0.4$ (Ref. 5).

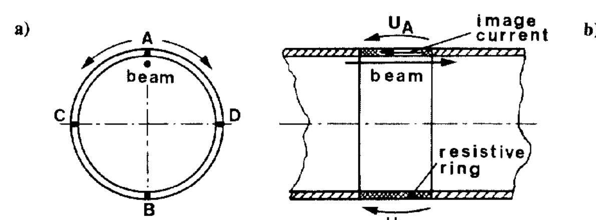

Fig. 5

3. Signal Propagation on the Lossy, Transverse Ring Line

3.1 Low-Frequency Limit

3.1.1 Low-frequency limit for the difference signal. Figure 5a shows the vacuum chamber with the beam in the extreme position near point A. Figure 5b is a section through A and B. The induced signal U_A generated in point A immediately starts to propagate to point B on the two resistive ring lines via CB and DB. If the travelling signals can be sufficiently damped so that no signals appear in point B, then the difference

$$\Delta U = U_A - U_B \tag{10}$$

can be used to determine the beam position. This is possible for a lossy line above a certain frequency limit. This limit will be determined below.

The general line propagation constant[6]

$$\gamma = \alpha + j\beta = \sqrt{(R + pL)(G + pC)} \tag{11}$$

(R = resistance, L = inductance, G = conductance, C = capacitance per unit length of line; $p = j\omega$) for $R \ll pL$ and $G \gg pC$ simplifies to

$$\gamma = \alpha + j\beta = \sqrt{pLG} = \sqrt{\omega LG/2}\,(1 + j) \tag{12}$$

and

$$\alpha = \beta = \sqrt{\omega LG/2}\ . \tag{13}$$

From points A to B (Fig. 5a) there are two lines of length ℓ in parallel, forming an open-ended double line; thus the output signal U_B generated by an input signal U_A is[6]

$$U_B = U_A/\cosh\gamma\ell\ , \tag{14}$$

and, with Eqs. (10) and (12),

$$\Delta U/U_A = 1 - \{1/\cosh[(1 + j)\alpha\ell]\}\ . \tag{15}$$

At the lower-frequency limit where the difference voltage $\Delta U = U_A - U_B$ is 3 dB attenuated with respect to U_A,

$$|\Delta U| = |U_A - U_B| = |U_A/\sqrt{2}|\ . \tag{16}$$

Combining Eq. (16) with Eq. (15) gives

$$|1 - \{1/\cosh[(1 + j)\alpha\ell]\}| = 1/\sqrt{2} \tag{17}$$

with the solution[5]

$$\alpha\ell = 0.93\ . \tag{18}$$

Inserting Eq. (18) in Eq. (13) we get

$$0.93 = \sqrt{\omega_c LG/2}\cdot\ell \tag{19}$$

and the lower cut-off frequency

$$f_L = \omega_c/2\pi = (0.93)^2/LG\ell^2\pi\ , \tag{20}$$

or with $\ell = d\pi/2$ (d = diameter of the chamber)

$$\boxed{f_L = 0.111/LGd^2\ .} \tag{21}$$

The lower cut-off frequency of the difference signal decreases inversely to the product LGd^2. Ex.: d = 10 cm; L = 3.5 nH/cm; G = 1/30 Ω·cm → f_L = 9.51 MHz.

3.1.2 The low-frequency limit of the sum signal. This limit would be zero without external closure of the gap.

3.2 Upper-Frequency Limit

Figure 6 shows the resistive ring line of impedance Z with the distributed current sources (arrows)

$$di = q(\ell)\,d\ell\ . \tag{22}$$

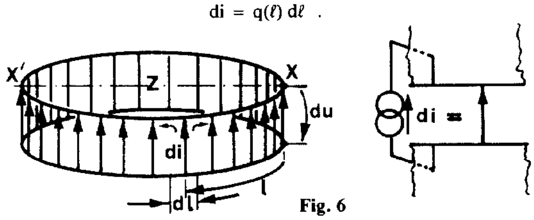

Fig. 6

From each source di alone, there is one wave going to the left and one to the right (each di/2). The voltage generated at the output point x by the source di/2 at a distance ℓ is

$$du = Z\,e^{-\gamma\ell}(di/2)\ . \tag{23}$$

As each current source can contribute not only from distance ℓ but also from $\ell + N\lambda$ (λ = circumference, N = 0, 1, 2, ..., ∞), integration to infinity is required. Assuming a symmetric current density distribution $q(\ell)$ with respect to x–x' (beam on the x axis), the left-going and right-going waves give the same contribution, i.e. by superposition

$$\boxed{U = Z\int_0^\infty e^{-\gamma\ell}q(\ell)\,d\ell\ .} \tag{24}$$

3.2.1 A centred beam with current I has a constant charge and current distribution versus ℓ ($\phi = \ell$ for r = 1):

$$q(\ell) = I/\lambda\ , \tag{25}$$

and generates an output voltage [Eq. (24)]

$$U(p) = Z\cdot(I/\lambda)\cdot\int_0^\infty e^{-\gamma\ell}\,d\ell\ ; \tag{26}$$

integrated, it gives

$$\boxed{U(p) = Z\cdot(I/\lambda)\cdot(1/\gamma)\ .} \tag{27}$$

Inserting into Eq. (27), the characteristic impedance[6]

$$Z = \sqrt{(R+pL)/(G+pC)} \tag{28}$$

and the propagation constant γ of Eq. (11), the factor (R + pL) cancels and

$$U(p) = I(p)/[(G+pC)\lambda] = [I(p)/G\lambda]\,\{1/[1+p(C/G)]\}\ . \tag{29}$$

Equating the real and imaginary part of the denominator leads to the high-frequency limit for a centred beam

$$\boxed{f_{HC} = \omega_{HC}/2\pi = G/2\pi C\ .} \tag{30}$$

Example: C = 1 pF/cm; G = 1/30 Ω·cm; → f_{HC} = 5.3 GHz.

A Dirac current input pulse delivers an output signal which decays with T = C/G = 30 ps time constant.

3.2.2 An off-centre beam with the current distribution of Eq. (1) and r ≠ 0 delivers with Eq. (24) a less simple integral.

But considering the propagation time $t_p = d\beta/d\omega$ (for distance ℓ in Fig. 6) which determines the rise-time of the output signal U, we find[5] that the effective length of the contributing lines from left and right shrinks with frequency. As a result, the high frequency limit of the difference signal is approximately equal to that of the sum signal, i.e.

$$\boxed{f_{HD} \approx f_{HC}\ .}$$

3.3 Gap Line with Lumped Resistors

Replacing the uniformly conducting ring by many equal lumped resistors, evenly distributed in a gap of the vacuum chamber, offers some advantages:

i) The impedance of the four connection cables can be included in the resistors.

ii) The inductance ℓ_s of the resistors r_s can be used to emphasize the high frequencies, which allows compensation for cable losses.

iii) Simpler manufacture.

However, the introduction of the series induction ℓ_s to the resistors r_s changes the equations: G must be replaced by $1/(r_s + p\ell_s)$.

Furthermore, the monitor gap should be closed to the exterior to avoid interactions (Fig. 7). This introduces a further time constant $T_1 = L_p/R$.

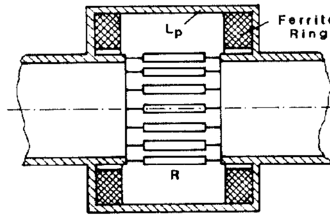

Fig. 7

The final transfer function for the sum signal (derived in ref. 5) is

$$\boxed{F_{1s}(p) = U(p)/I(p) = R\,[(1+pTQ^2)/(1+pT+p^2T^2Q^2)]\,[pT_1/(1+pT_1)]} \tag{31}$$

with $R = r_s/\lambda$, $L_s = \ell_s/\lambda$, $C_p = C\cdot\lambda$, $T_1 = L_p/R$, $T = R\cdot C_p$, and $Q = \sqrt{L_s/C_p}/R$ (λ = circumference of chamber, L_p = inductance of external closure with ferrite). The transfer function for the difference signal is

$$\boxed{F_{1d}(p,x) = \Delta U(p)/I(p) = K_{1d}(x)F_{1s}(p)[1 - (1/\cosh\sqrt{pT_c})]} \tag{32}$$

with K_{1d} = position dependence ($K_{1d} \propto x$), and $T_c = LG\cdot(\lambda/2)^2$.

4. Signal Transmission and Optimization

The signals appearing at the four axis points are connected to wide-band hybrids H which deliver the sum and difference signals (Fig. 8). Three filters Fi correct these signals before they are transmitted over 100 m of high-quality cables (7/8-inch Flexwell, 50 Ω) to the observation point.

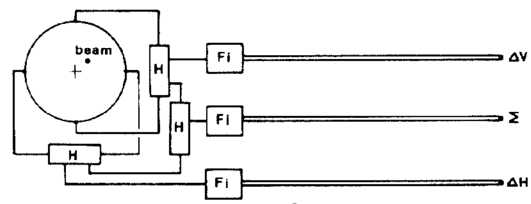

Fig. 8

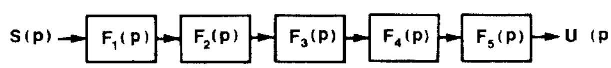

Fig. 9

Figure 9 shows a block diagram of the transmission with the transfer function

$$F(p) = U(p)/S(p) = F_1\cdot F_2\cdot F_3\cdot F_4\cdot F_5\ , \tag{33}$$

where for the

monitor:	F_1, see Eqs. (31) and (32);
hybrid:	$F_2 = (pT_2)/[(1+pT_2)(1+pT_3)]$ (approximated) ,
filter:	$F_3 = 1/[2+Y(\varrho+Z) + (\varrho/Z)]$;
	$\varrho = R_2/(1+pT_5)$, $Y = pC_1/(1+pT_4)$,
	$T_4 = R_1C_1$, $T_5 = R_2C_2$
	belonging to the circuit of Fig. 10, and
cable:	$F_4 = \exp(-\sqrt{pT_0})$; $T_0 = (\alpha\ell)^2/\pi f$,[8]
oscilloscope:	$F_5 = \exp[(pT_6)^2]$ (approximated).

More details have been given elsewhere.[5]

The difference between F(p) and an ideal, theoretical transfer function

$$T(p) = U(p)/S(p) = K\,e^{-p\tau + j\psi} \quad \text{(circle in Fig. 11)}\ ,$$

which has constant group delay τ and amplitude K (ψ = initial phase), is the complex error vector

$$\epsilon(p) = F(p) - T(p) \tag{34}$$

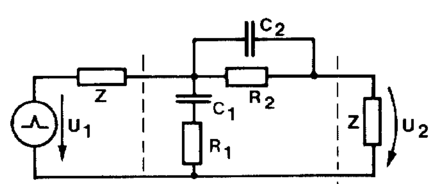

Fig. 10

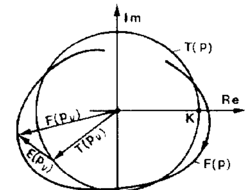

Fig. 11

shown in Fig. 11. The sum of the modulus $|\epsilon(p)|^2$ at many frequencies m in the desired range is a measure of the total error:

$$E = \sum_{\nu=1}^{m} |\epsilon(j\omega_\nu)|^2 = \sum_{\nu=1}^{m} |F(p_\nu) - T(p_\nu)|^2 \qquad (35)$$

which is a real function of all known and unknown variables, has been minimized with the computer program MINUIT[7] and thus led to the optimum values of the filter elements. There exist several optima. (Example: (Fig. 10) $R_1 = 179\ \Omega$; $R_2 = 17.1\ \Omega$; $C_1 = 205$ pF; $C_2 = 47.3$ pF; $Q = 1.5$ for the sum channel.)

The output of the different optimum settings was studied in the time domain with the LAPLACE program[8] for different input signals S(p) (Fig. 9):

i) Dirac pulse $S_1(p) = 1$
ii) rectangular pulse $S_2(p) = [1 - \exp(-p\tau)]/p$; ($\tau$ = pulse length)
iii) triangular pulse $S_3(p) = [1 - \exp(-p\cdot\tau/2)]^2/p^2$
and the best setting of the parameters was retained.

5. Mechanical Design

Figure 12 shows the monitor with three 180° hybrids (ANZAC H9, 2 MHz–2 GHz). The hybrids are connected to the resistor ring by four coaxial cables (RG58) of equal length. The ring is composed of 96 resistors, 32 in parallel of 3 in series on the periphery. The three series resistors ($3 \times 10\ \Omega$, MF) bridge the gap of 4 cm width. A ceramic tube ($\varnothing$ = 100 mm) of 5 mm thickness makes the gap vacuum-tight. The outer cavity contains two ferrite rings (2E8 PHIL).

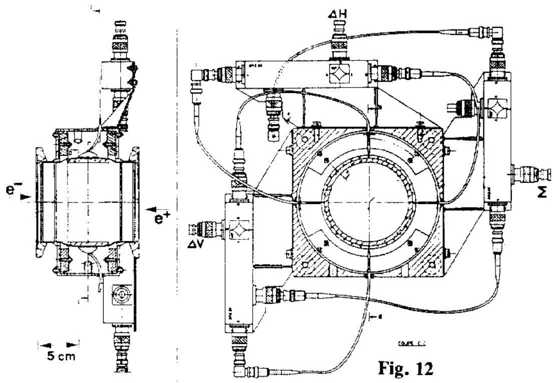

Fig. 12

6. Test-Bench Results

The measurement device is a 3 m long brass tube ($\varnothing$ = 100 mm) into which the monitor is inserted. Rectangular flanges at both ends allow linear transverse displacements of an inner wire (1 mm) or tube ($\varnothing$ = 20 mm). A fast-pulse or step-pulse generator feeds the inner conductor through one flange. The reflections at the flanges are sufficiently well separated from the signals by the relatively long propagation time in the tube (time filtering).

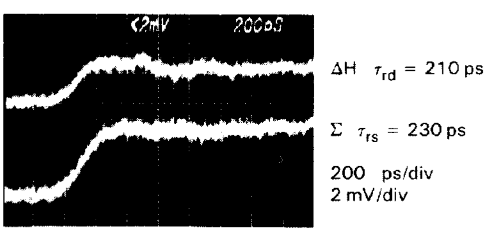

Fig. 13

Figure 13 was obtained with a 35 ps rise-time pulse generator (TDR sampler S52/7S12 TEK). It shows the Δ and Σ signals from the monitor, via hybrids, filter and 100 m cable attenuation (200 ps/div.). The rise-time corresponds to about 1.5 GHz.

7. Results with the Beam

Typical bunch signals of the monitor, installed in the e^+/e^- accumulator (EPA), are shown in Fig. 14 (oscilloscope: TEK 7A29/7104; cable length = 100 m).

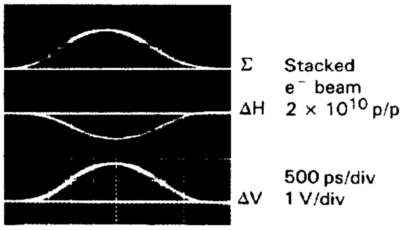

Fig. 14

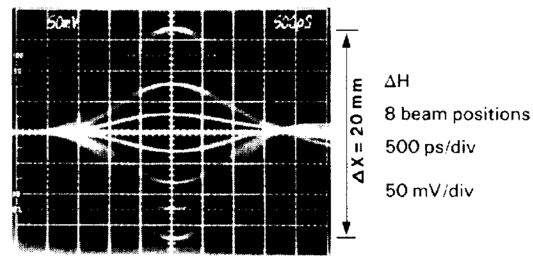

Fig. 15

Figure 15 demonstrates eight superimposed horizontal beam-position signals (range = 20 mm) obtained by varying a dipole current.

Figure 16 shows a 'mountain-range' display of a coupled bunch instability which starts at $\approx 2 \times 10^{11}$ total particles for eight circulating bunches, and produces, at 4×10^{11} particles (Fig. 16), coherent phase oscillations as displayed. (The noise on the base lines comes from the 'mountain-range' trigger unit.)

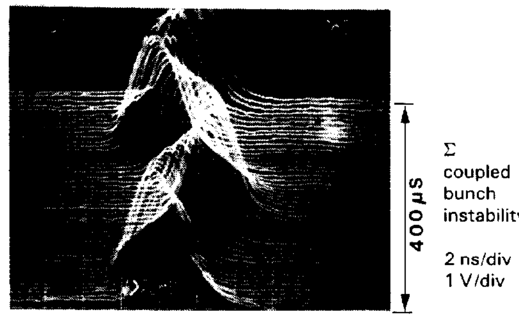

Fig. 16

8. Characteristics

The characteristics of the total system, i.e. monitor, hybrids, filters, and 100 m cables, are as follows:

- Bandwidth (intensity)	2.7 MHz–1.5 GHz
- Bandwidth (position)	9.4 MHz–1.6 GHz
- Sensitivity (beam current)	1.26 mV/mA
- Sensitivity (intensity, 4σ = 2.8 ns)	1.1 V/10^{10} particles per bunch
- Resolution (intensity)	$< 5 \times 10^6$ particles per bunch
- Total gap resistance	0.94 Ω
- Sensitivity (position)	40 ΔU/ΣU mm
- Resolution (position at 10^9 particles per bunch)	0.5 mm
- Linearity error for $\lvert r\rvert \leq 20$ mm	< 5%
- Coupling impedance $\lvert Z/n\rvert$	0.2 Ω
- Rise-time (intensity signal)	230 ps
- Rise-time (position signal)	210 ps

Closing Remarks

- The lower-frequency limit f_L of the position signal could be further decreased by increasing the monitor aperture, the inductance, and/or the conductance of the transverse gap line. Doubling the diameter would reduce f_L by a factor of 4.
- The inductance L of the gap line increases with the gap width. Trials to increase L by ferrite loading of the gap have been less effective.[5]
- The high-frequency limits are, for R = 0.94 Ω, essentially given by the hybrids, the transmission cables, and the cable connections to the gap.

Acknowledgements

It is a pleasure to thank A. Krusche and H. Kugler for stimulating discussions, D. Fiander for his support, M. Corcelle for the mechanical design, and P. Pelletier for the assembly of the monitors.

References

[1] G. Schneider, The new pick-up electrodes for the CPS, PS/INT.RF 65-9 (1965).

[2] R.T. Avery et al., Non-intercepting monitor of beam current and position, UCRL-20166 (1971).

[3] G. Schneider, Messwerterfassung und Übertragung zur Strahllagebestimmung am 28 GeV ... , Thesis, 1971, Techn. Universität, Hannover, p. 12.

[4] R. Bossart, Analysis and performance of the wall-current monitor for the SPS, Lab II-Co/Int/BM 75-2 (1975).

[5] G.C. Schneider, 1.5 GHz wide-band beam-position and intensity monitor for the EPA, CERN/PS 87-9 (1987).

[6] Howard W. Sams et al. (eds.), Reference Data for Radio Engineers (ITT publication 1972), p. 22-23.

[7] F. James and M. Roos, Function minimization program MINUIT, D506, CERN Program Library, 1978.

[8] H.H. Umstätter, Program LAPLACE, unpublished.